Available online at www.sciencedirect.com

ScienceDirect

journal homepage: www.elsevier.com/locate/he

CO_2 reduction on Cu/C used as a cathode in a polymeric electrolyte reactor - Fuel cell type

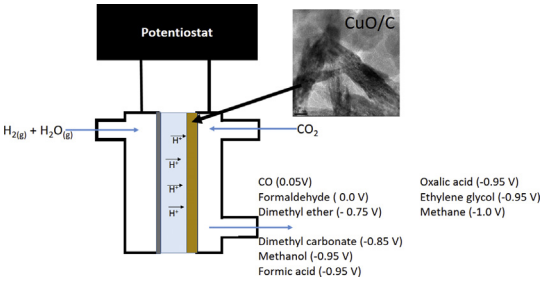
*Mariana Lima, Camila M. Godoi, Monique C.L. Santos, Julio Nandenha, Almir O. Neto, Rodrigo F.B. De Souza**

Centro de Célula a Combustível e Hidrogênio Instituto de Pesquisas Energéticas e Nucleares, IPEN/CNEN-SP, Av. Prof. Lineu Prestes, 2242 Cidade Universitária, CEP 05508-000, São Paulo, SP, Brazil

HIGHLIGHTS

- CO_2RR on polymeric electrolyte reactor.
- Mapping CO_2 reduced products for onset potential and tracing a reaction pathways.
- CO_2RR on Cu/C to C1–C2 products.

GRAPHICAL ABSTRACT



ARTICLE INFO

Article history:
Received 20 August 2021
Received in revised form
1 November 2021
Accepted 2 November 2021
Available online 23 November 2021

Keywords:
CO_2RR
Reactor type fuel cell
CO_2 to products
CO_2 activation over cu

ABSTRACT

CO_2 is one of the leading greenhouse gases, so studies that turn this gas into higher value-added products, that function as simpler and cheaper hydrogen stores, as an alcohols, are extremely important. In this work we using a polymeric Electrolyte Reactor– fuel cell type supplied with H_2 on platinum anode and dry CO_2 in the cathode with a copper-carbon electrocatalyst. Copper nanoparticles supported on carbon Vulcan XC72 were produced by the sodium borohydride reduction method. The XRD revealed the presence of two different phases, CuO and Cu_2O. In addition, the TEM images revealed agglomerates presence. The water, formaldehyde, methanol, methane, formic acid, dimethyl ether, oxalic acid, dimethyl carbonate, and ethylene-glycol were observed by differential mass spectroscopy on line with the reaction and the onset potential for each product and these results were confirmed by infrared spectroscopy – ATR-FTIR setup. This work showed the mapping CO_2 reduced compounds for onset potential proposing some contributions to the literature.

© 2021 Hydrogen Energy Publications LLC. Published by Elsevier Ltd. All rights reserved.

* *Corresponding author.*
E-mail address: souza.rfb@gmail.com (R.F.B. De Souza).

https://doi.org/10.1016/j.ijhydene.2021.11.008

0360-3199/© 2021 Hydrogen Energy Publications LLC. Published by Elsevier Ltd. All rights reserved.

Introduction

CO_2 is one of the leading greenhouse gases and great efforts have been made to reduce emissions, and finding ways to capture the gas [1,2]. Another strategy to mitigate this environmental issue is to convert carbon dioxide into value-adding chemicals, fuel-based products or molecules for hydrogen storage [3,4]. Unfortunately, this is not an easy task. Carbon dioxide is a linear molecule with two equivalent C=O bonds, in which their energy equals 750 kJ mol^{-1}, whereas a generic C–C, C–O and the C–H bond has an energy equal to 336 kJ mol^{-1}, 327 kJ mol^{-1}, 336 kJ mol^{-1} respectively [1].

Despite this difficulty, several chemical ways have been studied to enhancing the CO_2 reduction reaction, as a photocatalysis, thermal reform and electrochemical. The electrochemical paths are entirely appropriate because they can be carried out in mild conditions, such as in photocatalytic reactors [5,6], but with the advantage of modulating the energy to be applied by an external system [7].

The conversion by electrochemical routes has been improved over time, managing to decrease the overpotentials for the reaction to occur, followed by two different strategies catalysis and the other on reactors [8].

For electrocatalysis in which the main studies deal with composition, morphology, preferential crystallographic face, addition of functional groups and oxidation states [9–13]. Among the electrocatalysts used for the CO_2 Reduction Reaction (CO_2RR), copper has been demonstrated to be very promising; some authors attribute this activity to the high capacity of producing hydrocarbon products [12,14]. As suggested by Wuttig [15] and replying by Vasile [16] that cooper presents moderate adsorption of CO and this makes it possible to produce more complex compounds as a methanol [17], methane [13], ethanol [18], formates [19] and others [20] important chemicals feedstock, and molecules for hydrogen storage for energy applications [21–23].

On the other hand, different reactors designs have been worked, these reactors can be based on liquid electrolytes [9,11], polymeric electrolytes [24–26] or a mixture of both types to favor some mass transport or selectivity for products [18]. Electrodes and ways to diffuse gas are also widely addressed [9,27], however, there is not yet a standard to be followed as it occurs in several other electrochemical devices such as fuel cells for example [24–26].

Some reactors presented in the literature present architecture very similar to that of proton-exchanging fuel cells [24], the compartment cathodic and anodic chemistry are separated by a polymeric electrolyte membrane (PEM), and the flow of ions while attenuating product crossover. Highly-porous gas diffusion layers (GDLs) support the catalyst and promote prolonged contact between CO_2 molecules and the electrocatalyst during electrolyte contact. Also, in cathodic chamber the CO_2 can be delivered with a solution [28] or in the gas phase [25,26]. Some of the advantages of using polymeric electrolyte, is associated to the low operating temperature, the mechanical and chemical resistance in comparative than solid electrolyte [28,29].

In recent years, Gutiérrez-Guerra et al. [30] reduced CO_2 using a one proton exchange membrane reactor (PEM-R) like a fuel cell at a temperature of 110 °C, this reactor used Cu-Carbon as a cathodic catalyst and a polybenzimidazole (PBI) electrolyte membrane doped with H_3PO_4, where the acetaldehyde was the most common product (85% selectivity). Pérez-Rodríguez [31], works with a PEM-R using Nafion with electrolyte and a Fe/C as a cathode, presented that the higher current density due to the formation of H_2 by the reduction of water, while the conversion of CO_2 could be favored in the Fe electrode, both in an acidic medium and in the gaseous phase. This work was the first to map the products of CO_2 reduction reaction in potential function using a polymeric electrolyte reactor – fuel cell type, where it was utilized a proton exchange membrane at mild conditions on Cu/C and correlating the onset potential with the product obtained by differential mass spectrometry associated with FTIR spectroscopy performed in an ATR accessory.

Experimental

Cu/C catalyst was produced by the $NaBH_4$ reduction method, with 20% of the metallic charge and then supported in Vulcan XC72 carbon. The $CuCl_2 \cdot 2H_2O$ (Aldrich) salt was used as a metal source. The carbon Vulcan was dispersed in a solution containing 20 wt % Cu ions. This solution was sonicated for 10 min, and then the reducing agent $NaBH_4$ solution mixture (ratio 5:1 $NaBH_4$: metal ions) was added in the support + metal solution. This final solution was kept under stirring for 1 h at room temperature, so all the metal salts could be reduced. After 1 h, the final solution was filtered, washed with ultrapure water, and dried at 70 °C for 2 h [32].

The X-ray diffraction pattern of Cu/C was obtained using Rigaku Miniflex II with CuKα radiation source in the scan range of 2θ from 20° to 90° at 2° min^{-1}. The electron microscopy images were obtained using a transmission electron microscope (TEM) model JEM-2100 operated at 200 keV.

The polymeric electrolyte membrane reactor PER–FC–type was prepared using a cathode electrode composed of a diffuse layer and a catalytic layer of 1 mg copper per cm^{-2}. Moreover, it was used 5% Nafion® 117 membrane solution and isopropyl alcohol. The anode electrode was made in the same way, but using Pt/C (Basf ®) instead of Cu/C. The polarization curves were obtained using an Autolab PGSTAT 302 N potentiostat with a current booster. The unit cell with stainless steel plates for serpentine fuel delivered electrical work as a reactor. The carbon dioxide flow on the cathode surface was 10 mL min^{-1} with a 25 °C controlled humidifier bottle and with a flow delivery of 120 mL min^{-1} of H_2 on the anode. The humidifier bottle was heated up to a temperature of 85 °C.

The polymeric electrolyte reactor experiments were assisted by on-line differential mass spectroscopy (DMS) coupled to the reactor's anodic effluent output (Fig. 1). The DMS setup was described by Ramos [7]. The products of the cathodic reaction were also collected for 60 s in vials with water and hexane with increments of 50 mV and analyzed by ATR-FTIR performed in an ATR accessory (MIRacle with a ZnSe Crystal Plate Pike®) installed on a Nicolet® 6700 FT-IR spectrometer equipped with an MCT detector cooled with liquid N_2. Absorbance spectra were collected in the ratio (A: A_0). A represents a spectrum at a given potential at the anode, and A_0 is the spectrum obtained at ultrapure water and hexane (Aldrich).

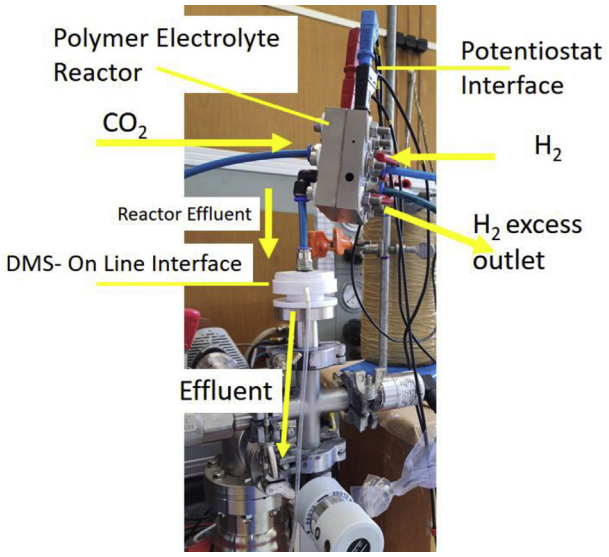


Fig. 1 – Setup experimental with polymeric reactor coupled in differential mass spectroscopy.

Results and discussion

For Fig. 2 shows the physical-characterization of Cu/C electrocatalyst. X-ray diffractogram pattern of Cu/C shows the presence of the crystalline plane (002) at approximately $2\theta = 25°$, associated with the hexagonal structure of the carbon support (JCPDS # 50–926), it is possible to observe copper nanoparticles in two phases CuO (JCPDS # 45–0937) with peaks at 35° (111), 46° (202) and 63° (113) and Cu_2O (JCPDS # 05–0667) phase convolved peak at ≈ 36° (111) and ≈62° (220), and an isolated peak at ≈ 39° (200). However, the existence of the metallic copper phase cannot be ruled out due to noise. Regarding the micrograph obtained by TEM illustrated in Fig. 1b), the nanoparticle's morphology was difficult to be observed due to high agglomeration; this could be due to the presence of higher Cu oxidation states [32,33].

Fig. 3a shows the j/V curves for PER-FC. During the CO_2RR, it is possible to observe that up to −0.25 V, the current tends to zero. Beyond that point, the curve tends to decrease, probably due to the reduction of copper oxides supported on carbon until it reaches stability around −0.5 V rapidly. Fig. 3 also shows the ionic currents (I_i) regarding the *m*/z ratios 44, 18, and 2, associated with CO_2, water, and H_2, respectively. For I_i (*m*/z = 44), it is observed that for potentials smaller than 0.1 V, the signal decreases while the potential is shifted to more negative values, indicating the reduction of CO_2 species.

For *m*/z = 18, it can be noticed that the profile remains relatively stable up to ≈ −0.8 V. Beyond this potential, the

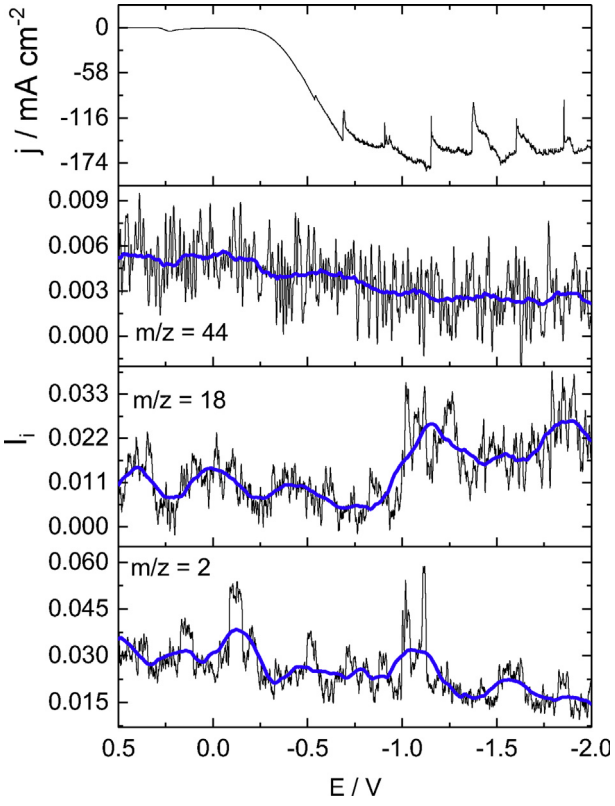


Fig. 3 – Electrochemical CO_2 reduction in Cu/C cathode at room temperature in the SER-FC with v = 1 mV s^{-1}, and the ionic currents measures for *m*/z 44, 18 e 2 (in blue line showed a 2-order polynomial regression).

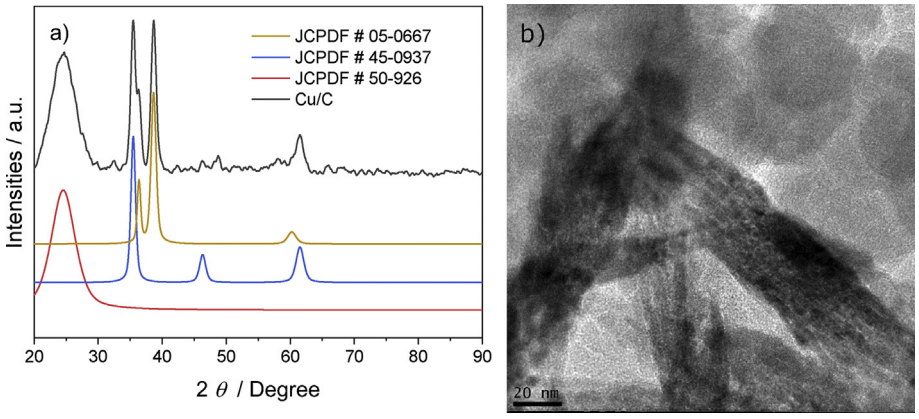


Fig. 2 – (a) X-ray diffractogram of Cu/C at 2° min^{-1} from $2\theta = 20°$ to 90°. (b) TEM micrography of the Cu/C catalysts prepared by the $NaBH_4$ reduction process.

current undergoes a slight increase and stabilizing at a new level; this behavior can be explained by the breaking of the C=O bond. Therefore, the O turns out to be available in an environment rich in protons. The signal for $m/z = 2$ shows a current decrease at approximately 0 V.

The CO_2 species were reduced and the I_i were observed for the m/z ratios 28, 30, 32, and 16, showed in Fig. 4. The CO_2RR products were carbon monoxide, formaldehyde, methanol, and methane. For $m/z = 28$ is possible to note large oscillations from 0.5 to 0.0 V, followed by an increase in intensity and subsequent decrease close to −1.0 V. These results agree with the 2152 cm^{-1} band attributed to CO formation [34] (Fig. 4b) in the range of 0.05 V to −1.0 V.

The $m/z = 30$ attributed to formaldehyde the signal is observed near 0 V, similar to the one observed for CO. The band at 1249 cm^{-1} (Fig. 4c) corresponding to the CH_2 rock formaldehyde vibration [35] can also be observed. For $m/z = 32$ attributed to methanol, a current increase is observed from 0.2 V, since methanol is only kept from −0.95 V up to −2.0 V through the band centered at ~1418 cm^{-1} (Fig. 4d) corresponding to OH bend [36]. The ratio $m/z = 16$ corresponding to methane has an increased profile from −1.0 V to −2.0 V with a significant jump in ~ −1.6 V and has a band at ~1530 cm-1 (Fig. 4e) corresponding to methane deg vibration [37].

According to Chen and coauthors [21], the first step to reduce CO_2 would be formate species, like formic acid. Due to

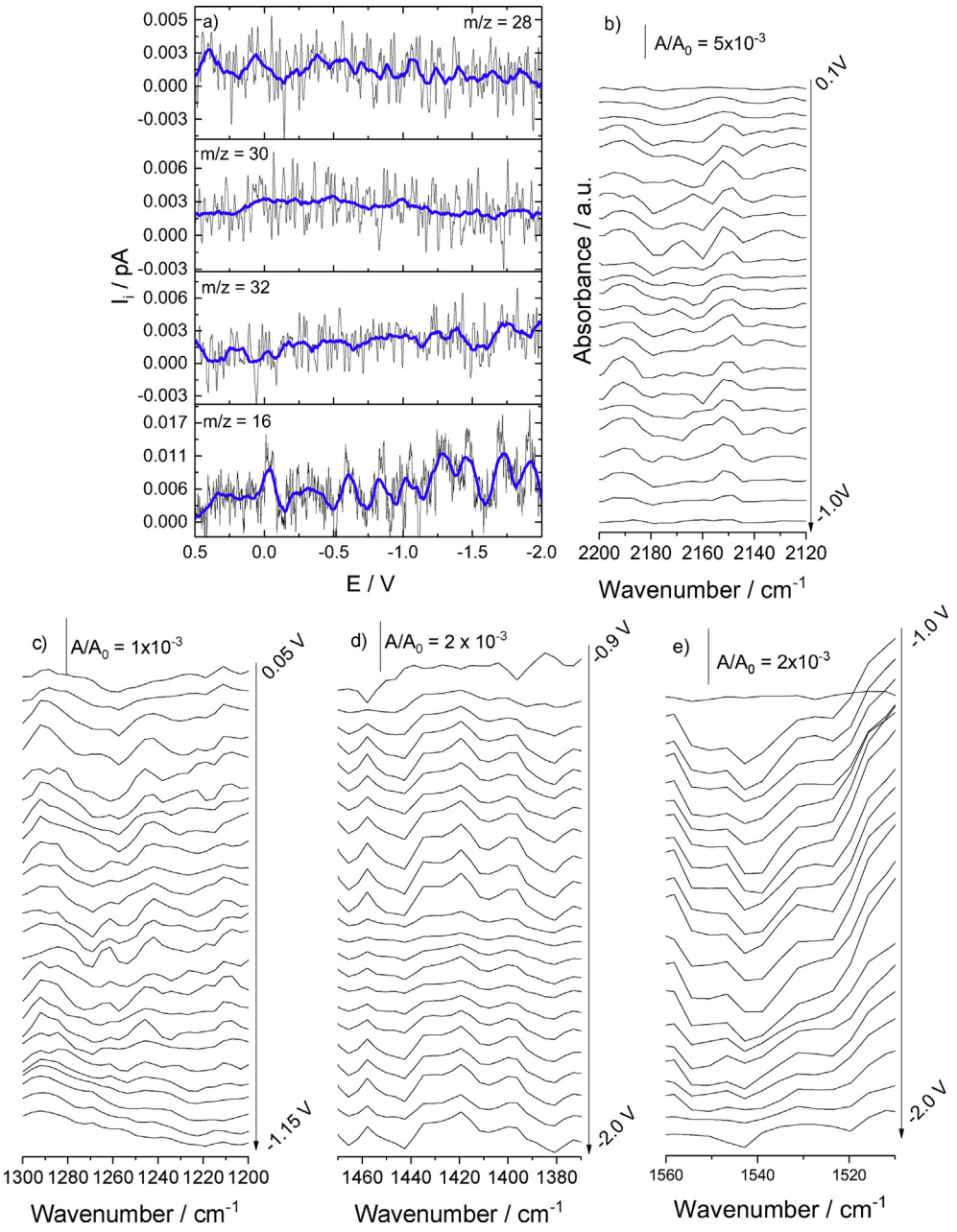


Fig. 4 – a) I_i* x potential for m/z 28, 30, 32 and 16; b); c); d) spectra of FTIR of PER-FC effluent collected in water; e) spectra of FTIR of PER-FC effluent collected in hexane.

the low energy in comparison the other products, probably the formates were not detected first, because they are still adsorbed on the catalytic sites. Fig. 5 shows the I_i for the *m/z* = 46, 90, 59, 60, 62, and 33.

The ratio *m/z* = 46 is more complex, as it may indicate formic acid, ethanol, dimethyl ether, and oxalic acid [38,39]. According to DFT calculations [21,40], formic acid would be the starting compound to be formed and from where the rest would be derived. The profile of I_i is increasing with the shift to more negative potentials with strong fluctuations across the range of potentials applied becoming clearer by observing the FTIR spectra. The band identifies formic acid at 1770 $cm^{-1,}$ which corresponds to C═O str [41] and is observed from −0.95 V persisting up to −2.0 V (Fig. 5c).

Some authors have used copper as a catalyst and reported that the main $RRCO_2$ product was ethanol [18,42]. However, none of these alcohol fragments is very different from the fragments of other possible products regarding mass spectrometry and FTIR spectroscopy. It was also not possible to observe the ethanol product by ATR-FTIR, and, due to the band's convolutions, their production cannot be disregarded.

The band corresponding to C–O–C *sym* stretch [43] of Dimethyl ether centered at 922 cm^{-1} (Fig. 5e) at −0.75 V agrees with one of the curve's peaks from I_i to *m/z* = 46, this could indicate that: i) the alcohol that gave rise to it has absorbed; ii) the process of two CO_2 molecules reducing in close places could give rise to this ether, as an extrapolation of the one proposed by Wuttig [15].

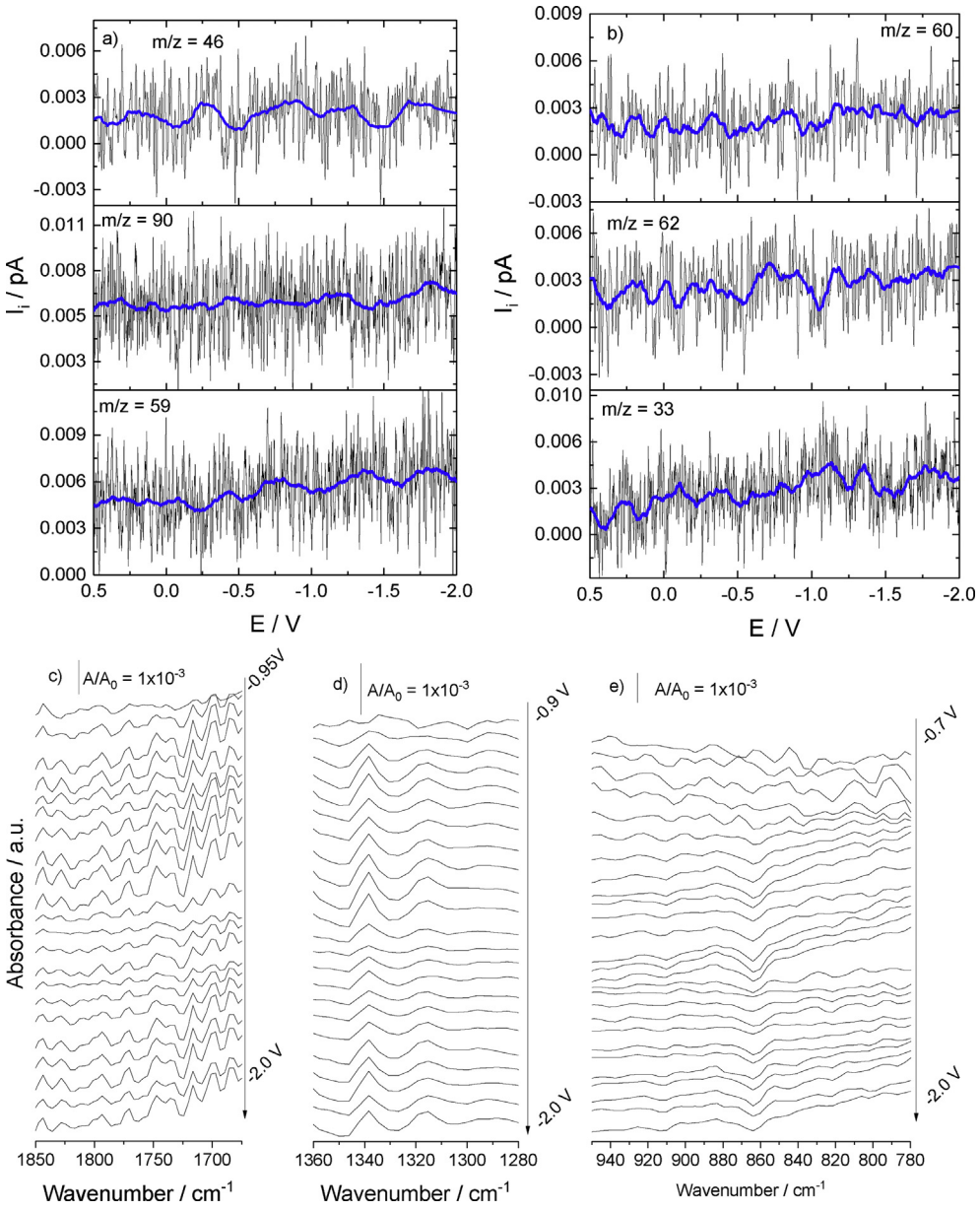


Fig. 5 – a) I_i x potential for *m/z* 46, 90, and 59; b) I_i x potential for *m/z* 60, 62, and 33; c); d); e) spectra of FTIR of PER-FC effluent collected in water.

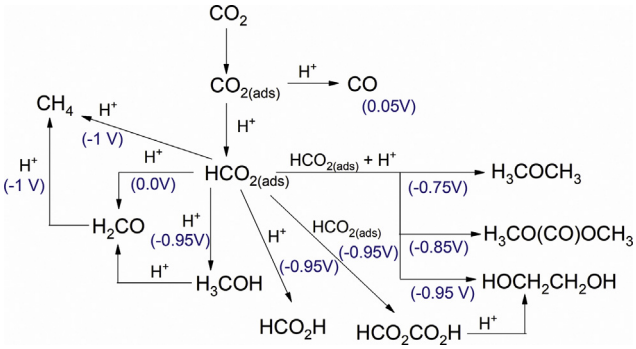


Fig. 6 – Reaction pathways of CO_2 reduction reaction on Cu/C in a PEM-R at mild condition.

Oxalic acid is one of the possibilities for $m/z = 46$ due to its main detection fragment [38]. However, it can also be observed at $m/z = 90$, a band assigned to C–O stretching of oxalic acid [44] centered at 1320 cm^{-1} (Fig. 5d) is detected at −0.95 V and increase the intensities until −2.0 V. Despite being a minority characteristic of dimethyl carbonate, the most abundant fragment is $m/z = 59$ and confirmed by the band of δOCO_2 (rock) at 794 cm^{-1} [45] from - 0.85 V (Fig. 5e) being a probable product of the addition of two methanol molecules to CO_2, as proposed by Zhao [46].

The acetic acid reported in the literature [42,47] would appear at $m/z = 60$. However, no specific bands were found in the FTIR spectra; nonetheless, for this m/z ratio, we also have the methyl-formate, identified by the band of CH_3 d-deform at 1443 cm^{-1} [48,49] (Fig. 4d), that exists in the same range as the detected I_i.

We also detected the fragments in $m/z = 62$ and 33 ethylene glycol confirmed by the ATR-FTIR spectra in 884 cm^{-1} corresponding to ρCH_2 [50]. In Fig. 5d, in the potential range of −0.95 to −2.0 V, the moderate adsorption of activated CO_2 is necessary to produce OCCO species [15], which justifies the formation of oxalic acid and in situations with less water availability. Still, with a high proton supply, ethyl glycol is also present makes it possible.

Based on the data collected by spectroscopy we propose these reaction steps, Fig. 6, seeing as the central point the HCO_2(ads), already mentioned in other works [21,40].

Conclusion

During the CO_2RR in a polymeric electrolyte reactor - fuel cell type over copper nanostructures composed by CuO and CuO_2 phases electrocatalyst, the water, formaldehyde, methanol, methane, formic acid, dimethyl ether, oxalic acid, dimethyl carbonate, and ethylene glycol were observed by differential mass spectroscopy on line with the reactor and confirmed by infrared spectroscopy. In these experiments it was possible to map the onset potentials for each species, and it was noted that some more complex species are detected at the outlet of the reactor before the appearance of simpler molecules that would give rise to. Indicating that these simpler molecules remained adsorbed on the catalytic layer forming the most complex species, causing delay in detection, the $HCO_{2(ads)}$ apointed as a central point of the reaction.

Declaration of competing interest

The authors declare that they have no known competing financial interests or personal relationships that could have appeared to influence the work reported in this paper.

Acknowledgements

The authors thank the CAPES (88882.315566/2019–01), CINE-SHELL (ANP)/FAPESP (2017/11937-4), CNPq (302709/2020-7) for the fellowships and the financial support this work.

REFERENCES

[1] Wang Y, He D, Chen H, Wang D. Catalysts in electro-, photo- and photoelectrocatalytic CO2 reduction reactions. J Photochem Photobiol C Photochem Rev 2019;40:117–49. https://doi.org/10.1016/j.jphotochemrev.2019.02.002.

[2] Cuéllar-Franca RM, Azapagic A. Carbon capture, storage and utilisation technologies: a critical analysis and comparison of their life cycle environmental impacts. Journal of CO2 Utilization 2015;9:82–102. https://doi.org/10.1016/j.jcou.2014.12.001.

[3] Ješić D, Lašič Jurković D, Pohar A, Suhadolnik L, Likozar B. Engineering photocatalytic and photoelectrocatalytic CO2 reduction reactions: mechanisms, intrinsic kinetics, mass transfer resistances, reactors and multi-scale modelling simulations. Chem Eng J 2021;407:126799. https://doi.org/10.1016/j.cej.2020.126799.

[4] Kim C, Dionigi F, Beermann V, Wang X, Möller T, Strasser P. Alloy nanocatalysts for the electrochemical oxygen reduction (ORR) and the direct electrochemical carbon dioxide reduction reaction (CO2RR). Adv Mater 2019;31:1805617. https://doi.org/10.1002/adma.201805617.

[5] Gusain R, Kumar P, Sharma OP, Jain SL, Khatri OP. Reduced graphene oxide–CuO nanocomposites for photocatalytic conversion of CO2 into methanol under visible light irradiation. Appl Catal B Environ 2016;181:352–62. https://doi.org/10.1016/j.apcatb.2015.08.012.

[6] Yaashikaa PR, Senthil Kumar P, Varjani SJ, Saravanan A. A review on photochemical, biochemical and electrochemical transformation of CO2 into value-added products. Journal of CO2 Utilization 2019;33:131–47. https://doi.org/10.1016/j.jcou.2019.05.017.

[7] Ramos AS, Santos MCL, Godoi CM, Oliveira Neto A, De Souza RFB. Obtaining C2 and C3 products from methane using Pd/C as anode in a solid fuel cell-type electrolyte reactor. ChemCatChem 2020;12:4517–21. https://doi.org/10.1002/cctc.202000297.

[8] Ghaib K, Ben-Fares F-Z. Power-to-Methane: a state-of-the-art review. Renew Sustain Energy Rev 2018;81:433–46. https://doi.org/10.1016/j.rser.2017.08.004.

[9] Wang Y, Shen H, Kjt Livi, Raciti D, Zong H, Gregg J, et al. Copper nanocubes for CO2 reduction in gas diffusion electrodes. Nano Lett 2019;19:8461–8. https://doi.org/10.1021/acs.nanolett.9b02748.

[10] Tao Z, Wu Z, Yuan X, Wu Y, Wang H. Copper–gold interactions enhancing formate production from electrochemical CO2 reduction. ACS Catal 2019;9:10894–8. https://doi.org/10.1021/acscatal.9b03158.

[11] Takatsuji Y, Nakata I, Morimoto M, Sakakura T, Yamasaki R, Haruyama T. Highly selective methane production through

electrochemical CO2 reduction by electrolytically plated Cu-Co electrode. Electrocatalysis 2019;10:29–34. https://doi.org/10.1007/s12678-018-0492-0.
[12] Yang D, Zhu Q, Chen C, Liu H, Liu Z, Zhao Z, et al. Selective electroreduction of carbon dioxide to methanol on copper selenide nanocatalysts. Nat Commun 2019;10:677. https://doi.org/10.1038/s41467-019-08653-9.
[13] Kim MK, Kim HJ, Lim H, Kwon Y, Jeong HM. Metal–organic framework-mediated strategy for enhanced methane production on copper nanoparticles in electrochemical CO2 reduction. Electrochim Acta 2019;306:28–34. https://doi.org/10.1016/j.electacta.2019.03.101.
[14] Spodaryk M, Zhao K, Zhang J, Oveisi E, Züttel A. The role of malachite nanorods for the electrochemical reduction of CO2 to C2 hydrocarbons. Electrochim Acta 2019;297:55–60. https://doi.org/10.1016/j.electacta.2018.11.124.
[15] Wuttig A, Liu C, Peng Q, Yaguchi M, Hendon CH, Motobayashi K, et al. Tracking a common surface-bound intermediate during CO2-to-Fuels catalysis. ACS Cent Sci 2016;2:522–8. https://doi.org/10.1021/acscentsci.6b00155.
[16] Vasileff A, Zhi X, Xu C, Ge L, Jiao Y, Zheng Y, et al. Selectivity control for electrochemical CO2 reduction by charge redistribution on the surface of copper alloys. ACS Catal 2019;9:9411–7. https://doi.org/10.1021/acscatal.9b02312.
[17] Huang W, Yuan G. A composite heterogeneous catalyst C-Py-Sn-Zn for selective electrochemical reduction of CO2 to methanol. Electrochem Commun 2020;118:106789. https://doi.org/10.1016/j.elecom.2020.106789.
[18] Theaker N, Strain JM, Kumar B, Brian JP, Kumari S, Spurgeon JM. Heterogeneously catalyzed two-step cascade electrochemical reduction of CO2 to ethanol. Electrochim Acta 2018;274:1–8. https://doi.org/10.1016/j.electacta.2018.04.072.
[19] Zhang X, Sun X, Guo S-X, Bond AM, Zhang J. Formation of lattice-dislocated bismuth nanowires on copper foam for enhanced electrocatalytic CO2 reduction at low overpotential. Energy Environ Sci 2019;12:1334–40. https://doi.org/10.1039/C9EE00018F.
[20] Otto A, Grube T, Schiebahn S, Stolten D. Closing the loop: captured CO2 as a feedstock in the chemical industry. Energy Environ Sci 2015;8:3283–97. https://doi.org/10.1039/C5EE02591E.
[21] Chen X, Lin Z-Z, Ju M, Guo L-X. Confined electrochemical catalysis under cover: enhanced CO2 reduction at the interface between graphdiyne and Cu surface. Appl Surf Sci 2019;479:685–92. https://doi.org/10.1016/j.apsusc.2019.02.132.
[22] Ye N, Jiang Z, Fang T. Probing the enhanced methanol electrooxidation mechanism by promoted CO tolerance on the Pd catalyst modified with TaN: a combined experimental and theoretical study. Int J Hydrogen Energy 2021. https://doi.org/10.1016/j.ijhydene.2021.09.056.
[23] Zhang Q, Shi C, Zhu E, Liu W, Liu K, Li Y, et al. Controllable electrodeposition synthesis of Pd/TMxOy-rGO/CFP composite electrode for highly efficient methanol electro-oxidation. Int J Hydrogen Energy 2021. https://doi.org/10.1016/j.ijhydene.2021.08.099.
[24] Weekes DM, Salvatore DA, Reyes A, Huang A, Berlinguette CP. Electrolytic CO2 reduction in a flow cell. Accounts Chem Res 2018;51:910–8. https://doi.org/10.1021/acs.accounts.8b00010.
[25] Wang G, Pan J, Jiang SP, Yang H. Gas phase electrochemical conversion of humidified CO2 to CO and H2 on proton-exchange and alkaline anion-exchange membrane fuel cell reactors. Journal of CO2 Utilization 2018;23:152–8. https://doi.org/10.1016/j.jcou.2017.11.010.
[26] Taifan W, Baltrusaitis J. CH4 conversion to value added products: potential, limitations and extensions of a single step heterogeneous catalysis. Appl Catal B Environ 2016;198:525–47. https://doi.org/10.1016/j.apcatb.2016.05.081.
[27] Del Castillo A, Alvarez-Guerra M, Solla-Gullón J, Sáez A, Montiel V, Irabien A. Sn nanoparticles on gas diffusion electrodes: synthesis, characterization and use for continuous CO2 electroreduction to formate. Journal of CO2 Utilization 2017;18:222–8. https://doi.org/10.1016/j.jcou.2017.01.021.
[28] Kortlever R, Shen J, Schouten KJP, Calle-Vallejo F, Koper MTM. Catalysts and reaction pathways for the electrochemical reduction of carbon dioxide. J Phys Chem Lett 2015;6:4073–82. https://doi.org/10.1021/acs.jpclett.5b01559.
[29] Li YC, Zhou D, Yan Z, Gonçalves RH, Salvatore DA, Berlinguette CP, et al. Electrolysis of CO2 to syngas in bipolar membrane-based electrochemical cells. ACS Energy Letters 2016;1:1149–53. https://doi.org/10.1021/acsenergylett.6b00475.
[30] Gutiérrez-Guerra N, Valverde JL, Romero A, Serrano-Ruiz JC, de Lucas-Consuegra A. Electrocatalytic conversion of CO2 to added-value chemicals in a high-temperature proton-exchange membrane reactor. Electrochem Commun 2017;81:128–31. https://doi.org/10.1016/j.elecom.2017.06.018.
[31] Pérez-Rodríguez S, Barreras F, Pastor E, Lázaro MJ. Electrochemical reactors for CO2 reduction: from acid media to gas phase. Int J Hydrogen Energy 2016;41:19756–65. https://doi.org/10.1016/j.ijhydene.2016.06.130.
[32] Godoi CM, Santos MCL, Silva AJ, Tagomori TL, Ramos AS, de Souza RFB, et al. Methane conversion to higher value-added product and energy co-generation using anodes OF PdCu/C in a solid electrolyte reactor: alkaline fuel cell type monitored by differential mass spectroscopy. Res Chem Intermed 2020;47:743–57. https://doi.org/10.1007/s11164-020-04296-4.
[33] Ji C, Yin S-N, Sun S, Yang S. An in situ mediator-free route to fabricate Cu2O/g-C3N4 type-II heterojunctions for enhanced visible-light photocatalytic H2 generation. Appl Surf Sci 2018;434:1224–31. https://doi.org/10.1016/j.apsusc.2017.11.233.
[34] Rezaei M, Sheybani-Deloui S, Moazzen-Ahmadi N, Michaelian KH, McKellar ARW. CO dimer: the infrared spectrum revisited. J Phys Chem 2013;117:9612–20. https://doi.org/10.1021/jp312337v.
[35] Liu J, Kim H-T, Anderson SL. Multiphoton ionization and photoelectron spectroscopy of formaldehyde via its 3p Rydberg states. J Chem Phys 2001;114:9797–806. https://doi.org/10.1063/1.1370943.
[36] Falk M, Whalley E. Infrared spectra of methanol and deuterated methanols in gas, liquid, and solid phases. J Chem Phys 1961;34:1554–68. https://doi.org/10.1063/1.1701044.
[37] Boudon V, Rey M, Loëte M. The vibrational levels of methane obtained from analyses of high-resolution spectra. J Quant Spectrosc Radiat Transf 2006;98:394–404. https://doi.org/10.1016/j.jqsrt.2005.06.003.
[38] Takegawa N, Miyakawa T, Kawamura K, Kondo Y. Contribution of selected dicarboxylic and ω-oxocarboxylic acids in ambient aerosol to the m/z 44 signal of an aerodyne aerosol mass spectrometer. Aerosol Sci Technol 2007;41:418–37. https://doi.org/10.1080/02786820701203215.
[39] Moshammer K, Jasper AW, Popolan-Vaida DM, Lucassen A, Diévart P, Selim H, et al. Detection and identification of the keto-hydroperoxide (HOOCH2OCHO) and other intermediates during low-temperature oxidation of dimethyl ether. J Phys Chem 2015;119:7361–74. https://doi.org/10.1021/acs.jpca.5b00101.
[40] Grabow LC, Mavrikakis M. Mechanism of methanol synthesis on Cu through CO2 and CO hydrogenation. ACS Catal 2011;1:365–84. https://doi.org/10.1021/cs200055d.

[41] Maçôas EMS, Lundell J, Pettersson M, Khriachtchev L, Fausto R, Räsänen M. Vibrational spectroscopy of cis- and trans-formic acid in solid argon. J Mol Spectrosc 2003;219:70–80. https://doi.org/10.1016/S0022-2852(03)00018-3.
[42] Hori Y, Takahashi I, Koga O, Hoshi N. Electrochemical reduction of carbon dioxide at various series of copper single crystal electrodes. J Mol Catal Chem 2003;199:39–47. https://doi.org/10.1016/S1381-1169(03)00016-5.
[43] Barnes AJ, Beech TR. The vibrational spectrum of the dimethyl ether-water complex. Chem Phys Lett 1983;94:568–70. https://doi.org/10.1016/0009-2614(83)85058-1.
[44] Back RA. The ultraviolet absorption spectrum of oxalic acid vapor. Can J Chem 1984;62:1414–28. https://doi.org/10.1139/v84-241.
[45] Katon JE, Cohen MD. The vibrational spectra and structure of dimethyl carbonate and its conformational behavior. Can J Chem 1975;53:1378–86. https://doi.org/10.1139/v75-191.
[46] Zhao T, Han Y, Sun Y. Novel reaction route for dimethyl carbonate synthesis from CO2 and methanol. Fuel Process Technol 2000;62:187–94. https://doi.org/10.1016/S0378-3820(99)00118-6.
[47] Genovese C, Ampelli C, Perathoner S, Centi G. Mechanism of C–C bond formation in the electrocatalytic reduction of CO2 to acetic acid. A challenging reaction to use renewable energy with chemistry. Green Chem 2017;19:2406–15. https://doi.org/10.1039/C6GC03422E.
[48] Susi H, Zell T. Vibrational spectra of methyl formate and deuterated analogs. Spectrochim Acta 1963;19:1933–45. https://doi.org/10.1016/0371-1951(63)80211-8.
[49] Wilmshurst JK. A vibrational assignment for methyl formate and methyl acetate. J Mol Spectrosc 1957;1:201–15. https://doi.org/10.1016/0022-2852(57)90023-1.
[50] Sawodny W, Niedenzu K, Dawson JW. The vibrational spectrum of ethylene glycol. Spectrochim Acta Mol Spectrosc 1967;23:799–806. https://doi.org/10.1016/0584-8539(67)80007-2.